coatings

MDPI

Article

Comparison of Cracking Resistance Evaluation Methods for Asphalt Mixtures and Influence of Test Parameters

Feng Huang [1,2], Can Jiang [1], Binbin Wang [1,2], Desheng Yang [1,2], Feng Xiong [1], Ke Li [3], Xin Yuan [1] and Haisheng Ren [4,*]

[1] China Merchants Zhixiang Road Technology (Chongqing) Co., Ltd., Chongqing 400067, China
[2] China Merchants Chongqing Communications Technology Research and Design Institute Co., Ltd., Chongqing 400067, China
[3] School of Intelligent Construction and Engineering Technology, Neijiang Vocational and Technical College, Neijiang 641000, China
[4] Intelligent Transportation System Research Center, Southeast University, Nanjing 211189, China
* Correspondence: ren_hs510@seu.edu.cn

Abstract

Cracking is one of the primary distresses in asphalt pavements. To select an appropriate cracking resistance evaluation method and clarify the influence of test parameters on evaluation indices, three types of AC-13 asphalt mixtures—base, SBS-modified, and rubber-modified—were tested at −10 °C using the indirect tensile (IDT), beam bending (BBT), and semi-circular bending (SCB) tests. The methods were compared using peak load, tensile strength, and fracture work, and subsequently the effects of key test parameters on the evaluation indices were investigated. The results show that, under the present procedures, the IDT test exhibits anomalous fracture behavior, crushing beneath the loading strips, and contradictory rankings between peak load and fracture work, indicating limited reliability for the evaluated indices. The BBT and SCB tests yield consistent rankings (rubber-modified > SBS-modified > base asphalt), agreeing with BBR test results; however, under the present procedures, the SCB test offers better discrimination and allows field core sampling and is therefore regarded as the more suitable method among the three for the mixtures and conditions examined. Fracture toughness (K_{IC}) and fracture energy (G_f) all decrease with increasing notch depth. K_{IC} increases with increasing loading rate and decreases with increasing temperature. G_f increases with loading rate under ductile fracture but peaks at 15 °C under lower rates, with an interaction between loading rate and temperature. At ambient temperature, K_{IC} is not a material constant and must be used under fixed temperature, loading rate, and notch depth. Accordingly, the conditions of 25 °C, 5 mm/min and a notch depth of 10–15 mm are proposed for the SCB test, subject to further validation. The findings provide a reference for selecting cracking resistance evaluation methods and optimizing test conditions.

Keywords: asphalt mixture; cracking resistance; semi-circular bending test; evaluation index; influencing factor

Check for updates

Academic Editor: Valeria Vignali

Received: 27 September 2026
Revised: 13 November 2026
Accepted: 16 November 2026
Published: 18 November 2026

Copyright: © 2026 by the authors. Licensee MDPI, Basel, Switzerland. This article is an open access article distributed under the terms and conditions of the Creative Commons Attribution (CC BY) license.

1. Introduction

Asphalt concrete pavements are widely used in various types of roads owing to their smooth surface, comfortable riding quality, and wear resistance, yet cracking remains one of their most common distresses [1–5]. Under traffic loading and temperature variations, early-initiated cracks further propagate into crack networks and may even cause structural

failure, constituting a major source of road maintenance and rehabilitation costs. Selecting asphalt mixtures with superior cracking resistance is an effective way to prevent cracking or delay crack propagation. Currently, according to relevant domestic and foreign standards, commonly used cracking resistance evaluation methods include the beam bending (BBT) test, indirect tensile (IDT) test, disk-shaped compact tension (DCT) test, and semi-circular bending (SCB) test [6]. However, specimen dimensions and test parameters differ among these methods, leading to discrepancies in evaluation results.

The BBT test is commonly used to assess the low-temperature performance of asphalt mixtures. Zhang [7] obtained extensive experimental data based on bending test methods and, combined with theoretical analysis, evaluated in detail the test methods for low-temperature cracking resistance of asphalt mixtures. Ge et al. [8] conducted low-temperature bending tests at 0 °C on an MTS810 material testing system and used grey relational analysis to examine the influence of various indices on the critical strain energy density; their results showed that the critical strain energy density index, a combination of critical bending strain and bending strength, provides a more scientific evaluation of low-temperature cracking resistance. Shen et al. [9] comprehensively evaluated the low-temperature performance of asphalt mixtures with different asphalt types, gradation curves, and aggregate compositions through low-temperature bending tests. Kim et al. [10] investigated the mode I fracture behavior of asphalt concrete using a single-edge notched beam (SENB) test. Wagoner et al. [11] improved the notch geometry, specimen dimensions, and test control mode and studied the variation in fracture energy with temperature using single-edge notched beam specimens.

The IDT test is regarded to date as one of the effective methods for predicting the low-temperature properties of asphalt mixtures, but it also has drawbacks: its testing and analysis are relatively complex, and the results rely on multiple assumptions. Yin et al. [12] evaluated the cracking resistance of asphalt mixtures using the indirect tensile strength test and calculated the cracking resistance coefficient Nflex by determining the ductile and brittle slopes; their results showed that test temperature significantly affects the Nflex factor, whereas the influence of loading rate is insignificant. Pi et al. [13] conducted a numerical simulation comparative study of asphalt splitting tests using ABAQUS software.

The SCB test originated from rock mechanics research and was subsequently introduced into the study of asphalt mixture cracking resistance by Krans [14]. Owing to its advantages of simple specimen preparation and good test repeatability, the SCB test has received increasing attention in recent years. Zeng et al. [15] analyzed the damage evolution and crack propagation behavior in SCB asphalt mixture specimens using numerical methods; Lancaster et al. [16] simulated the crack propagation process in the SCB test using the extended finite element method; Al-Qudsi et al. [17] performed cohesive fracture finite element simulations of asphalt mixtures at low temperatures based on the SCB test. Related studies [18–21] have used notched SCB tests to investigate the cracking resistance and potential influencing factors of different types of asphalt mixtures. Aliha et al. and Pirmohammad et al. [22,23] conducted low-temperature SCB tests under mode I, mode II, and mixed-mode loading conditions for different asphalt mixtures, studying the effects of temperature and air void content on fracture toughness. Huang [24] characterized the tensile strength of hot-mix asphalt mixtures using both SCB and IDT tests, and the results showed that the SCB test can significantly reduce loading-induced deformation and is more suitable for evaluating the tensile performance of hot-mix asphalt mixtures at high temperatures. On this basis, the SCB test has been incorporated into standardized procedures with different objectives: EN 12697-44 [25] determines the fracture toughness of notched SCB specimens at low temperatures under displacement control, whereas the Illinois Flexibility Index Test (I-FIT, AASHTO TP124) [26] is conducted at 25 °C and 50 mm/min with a 15 mm

notch and uses the flexibility index (FI), derived from fracture energy and the post-peak slope, as a rapid intermediate-temperature quality-screening indicator.

Although extensive research has been conducted on cracking resistance evaluation methods for asphalt mixtures both domestically and abroad, there remain numerous low-temperature fracture test methods and evaluation indices. In most cases, asphalt mixtures exhibit brittle material characteristics at low temperatures, but rubber-modified asphalt mixtures possess good low-temperature performance and show different characteristics under various test conditions. Relatively few studies have comprehensively evaluated different asphalt mixtures using multiple cracking resistance evaluation methods, and research that uses the cracking resistance performance of asphalt mixtures to corroborate the simplicity, reliability, repeatability, and sensitivity of fracture test methods is rarely reported. Furthermore, as a temperature-sensitive material, the fracture characteristics of asphalt mixtures are affected by different test parameters, making it particularly important to study the influence of test parameters on cracking resistance evaluation indices.

Accordingly, the present study first compares three cracking resistance evaluation methods—the IDT, BBT, and SCB tests—on three asphalt mixtures (base, SBS-modified, and rubber-modified). The comparison is made using three common indices (peak load, tensile strength, and fracture work), with BBR measurements and fracture-surface observations serving as corroborating evidence to assess the applicability of each method and identify the one with the most comprehensive advantages, extending earlier comparisons that were largely confined to two tests [24,27]. The study further examines the effects of temperature, loading rate, and notch depth on three fracture indices grounded in different concepts—J_{IC}, K_{IC}, and G_f. These indices have generally been investigated separately in previous studies [28,29], whereas in the present work they are derived from the same specimens and configuration, so the similarities and differences in their responses can be compared directly. Importantly, this side-by-side comparison is not intended to establish a hierarchy of the test methods; rather, it shows that the three conceptually different indices can respond differently, even in opposite directions, to the same change in temperature, loading rate or notch depth. Finally, the development of the fracture process zone with notch depth and loading rate is examined to interpret the dependence of the fracture energy on these factors and to provide a mechanistic basis for selecting test conditions.

2. Materials and Methods

2.1. Raw Materials

The asphalts used in this study were 70# base asphalt, SBS-modified asphalt, and rubber-modified asphalt. The SBS-modified asphalt was produced with a linear SBS modifier at a dosage of approximately 4.5% by mass of the base asphalt, and the rubber-modified asphalt was produced with crumb rubber from waste tires (about 40 mesh) at an external dosage of approximately 20% by mass of the base asphalt. The technical indices of the three asphalts were measured in accordance with the Standard Test Methods JTG E20-2011 [30] and JTG F40-2004 [31]; the results are presented in Tables 1–3. All technical indices of the three asphalts meet the specification requirements.

The coarse aggregate, fine aggregate, and mineral powder used in the test were derived from limestone. Their technical properties were tested in accordance with the requirements of Specification JTG E42-2005 [32], and the results met the specifications.

Table 1. Technical indices of 70# base asphalt.

Index		Unit	Technical Requirement	Test Result
Penetration (25 °C, 5 s, 100 g)		0.1 mm	60–80	64
Ductility (5 mm/min, 15 °C)		cm	100	>100
Softening point		°C	≥43	53
Density (15 °C)		g/cm^3	Measured	1.031
Solubility (trichloroethylene)		%	≥99.5	99.8
Flash point		°C	≥260	307
Rotational viscosity (Brookfield) (135 °C)		Pa·s	≤3	0.45
RTFOT	Mass change	%	±0.8	−0.12
	Residual penetration ratio	%	≥58	68
	Residual ductility (15 °C)	cm	≥4	7.5

Table 2. Technical indices of SBS-modified asphalt.

Index		Unit	Technical Requirement	Test Result
Penetration (25 °C, 5 s, 100 g)		0.1 mm	40–60	53
Ductility (5 mm/min, 5 °C)		cm	≥20	30
Softening point		°C	≥45	79
Density (15 °C)		g/cm^3	Measured	1.033
Solubility (trichloroethylene)		%	≥90	99.7
Flash point		°C	≥220	253
Rotational viscosity (Brookfield) (135 °C)		Pa·s	≤3	1.08
RTFOT	Mass change	%	±1.0	−0.26
	Residual penetration ratio	%	≥65	70
	Residual ductility (5 °C)	cm	≥15	18

Table 3. Technical indices of rubber-modified asphalt.

Index	Unit	Technical Requirement	Test Result
Penetration (25 °C, 5 s, 100 g)	0.1 mm	40–80	42
Ductility (5 mm/min, 15 °C)	cm	-	33
Softening point	°C	≥70	95
Dynamic viscosity at 60 °C	Pa·s	≥20,000	490,000
Elastic recovery	%	≥85	94

Table 3. *Cont.*

Index		Unit	Technical Requirement	Test Result
Segregation		°C	≤2.5	1.7
RTFOT	Mass change	%	±1.0	0.06
	Residual penetration ratio	%	≥65	85
	Residual ductility (5 °C)	cm	≥15	25

In this study, AC-13 asphalt mixtures were selected as the research object. All three asphalt mixtures adopted the same aggregate gradation, designed using the combined aggregate gradation method, with the gradation curve close to the median gradation to ensure that the mechanical properties and durability of the mixtures remain in a relatively good and stable state. The AC-13 gradation curve is shown in Figure 1.

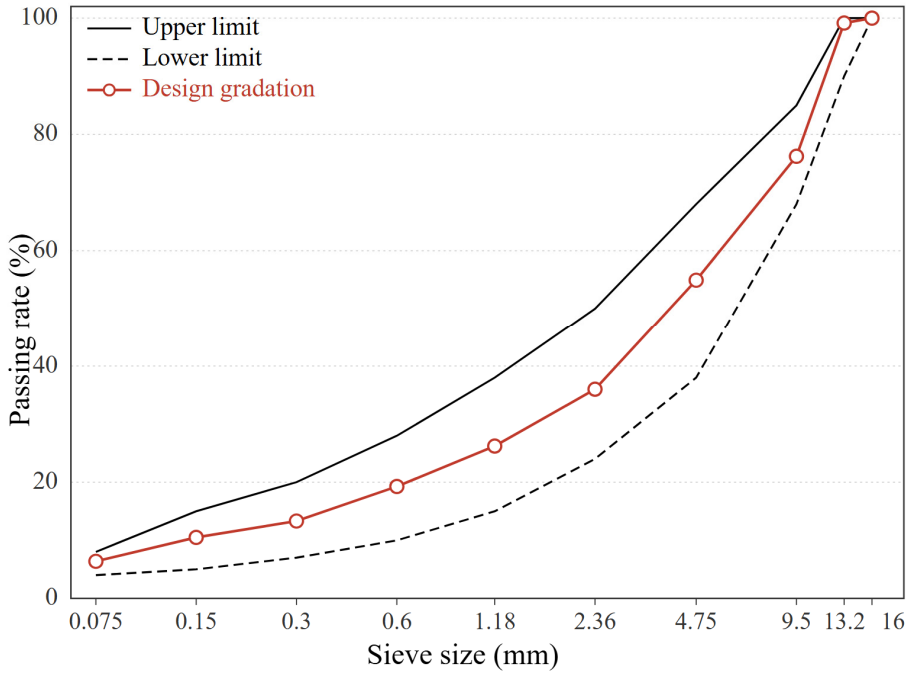


Figure 1. Aggregate gradation design curve [31].

Marshall mix design was performed in accordance with JTG F40-2004 to determine the optimum asphalt content and volumetric properties of the three mixtures, as summarized in Table 4. The Marshall-compacted specimens were used solely for mix proportioning. The specimens for the three fracture tests were then fabricated by methods suited to each geometry: IDT and SCB specimens were cut from cylinders (φ150 mm × 160 mm) compacted with a Superpave gyratory compactor (PINE), with the number of gyrations adjusted to attain the target air void of 4%, whereas BBT specimens were cut from roller-compacted slabs (see Sections 2.2.1–2.2.3). After compaction and cutting, the specimens were tested directly, without ageing or additional conditioning.

Table 4. Marshall mix-design results of the three AC-13 mixtures.

Mixture	OAC/%	Bulk Specific Gravity	Air Voids VV/%	VMA/%	VFA/%	Stability/kN	Flow/mm	Mixing Temperature/°C
Base asphalt mixture	5.0	2.431	4.0	14.4	69.1	10.5	2.5	140
SBS-modified asphalt mixture	4.9	2.425	3.9	14.5	70.5	13.3	2.7	165
Rubber-modified asphalt mixture	5.1	2.409	4.2	14.7	71.3	15.4	3.3	175

To evaluate the low-temperature performance of the three raw asphalts, bending beam rheometer (BBR) tests were conducted in accordance with ASTM D 6648. The specimen dimensions were 127 mm × 12.7 mm × 6.35 mm. A constant load of 980 mN ± 50 mN was applied for 240 s at −10 °C, and the stiffness modulus S and creep rate m-value at 60 s were recorded. The test results show that all three asphalts satisfy the requirements of $S < 300$ MPa and $m \geq 0.3$. The stiffness modulus follows the order base asphalt > SBS-modified asphalt > rubber-modified asphalt, while the m-value follows base asphalt < SBS-modified asphalt < rubber-modified asphalt. Comprehensive analysis indicates that the rubber-modified asphalt has the best low-temperature cracking resistance, followed by the SBS-modified asphalt, with the base asphalt being the poorest.

2.2. Low-Temperature Cracking Tests

To compare the applicability of different test methods in evaluating the low-temperature cracking resistance of asphalt mixtures, the IDT, BBT, and SCB tests were conducted on three types of asphalt mixtures. All three tests were performed at −10 °C, with at least three valid replicate specimens for each mixture and test method; the reported values are the mean values of the valid replicates. Before testing, the specimens were kept in a temperature-controlled chamber for 4 h to ensure uniform internal temperature. A SANS universal testing machine was used for loading, with a data acquisition rate of 32 Hz.

2.2.1. Indirect Tensile (IDT) Test

In the IDT test, a monotonic compressive load parallel to the vertical diametral plane is applied to a cylindrical specimen, as shown in Figure 2. The compressive load is distributed through curved loading strips at the interface to accommodate the radius of curvature of the specimen. The specimens were cored from rotary-compacted samples, with dimensions of φ100 mm × 40 mm (diameter × thickness). The loading strip width was 12.7 mm, and the inner curvature radius was 50.8 mm. The loading rate was 1 mm/min.

2.2.2. Beam Bending (BBT) Test

The BBT test adopts a three-point bending mode, in which a load is applied at the mid-span of a prismatic specimen until fracture failure, as shown in Figure 3. The specimens were cut from wheel tracking slabs formed by a roller compactor, with dimensions of 250 mm × 30 mm × 35 mm (length × width × height) and a span of 200 mm. The loading rate was 50 mm/min.



Figure 2. IDT test setup.



Figure 3. BBT test setup.

2.2.3. Semi-Circular Bending (SCB) Test

The SCB test setup consists of two support rollers at the bottom and one loading roller at the midpoint of the semicircular arc, as shown in Figure 4. Both the support points and loading head use rollers to reduce friction and simplify boundary conditions. The specimen geometry and loading arrangement were based on EN 12697-44 [25]: the specimens were cut from rotary-compacted samples with a diameter of 150 mm and a thickness of 50 mm; a prefabricated notch with a depth of 10 mm (notch width 1.5 mm) was cut at the bottom, the support roller spacing was 0.8 D, and the loading rate was 5 mm/min. The test was stopped when the load had fallen to approximately 100 N or when the specimen was completely fractured. Specimens were considered invalid if the crack tip at failure deviated from the specimen center by more than 0.1 D; non-conforming specimens were discarded and replaced, ensuring at least three valid replicate specimens for each condition.

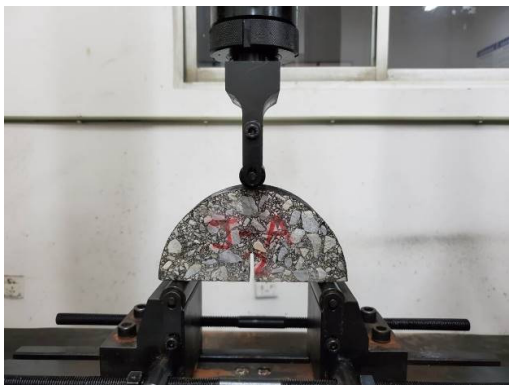


Figure 4. SCB test setup.

The three tests adopted unified evaluation indices: the peak failure load was measured directly from the test; the tensile strength was calculated using Equations (1)–(3); and the fracture work W_f, defined as the integral of the area under the load–displacement curve, reflects the total energy absorbed during the fracture process of the specimen.

$$R_T = 0.00628 P_{\max} / h_1 \tag{1}$$

$$R_B = \frac{3LP_{\max}}{2bh_2^2} \tag{2}$$

$$\sigma_{\max} = \frac{4.263 \times P_{\max}}{D \times t} \tag{3}$$

where R_T, R_B, and $\sigma_{\max}$ are the tensile strengths at failure of the IDT, BBT and SCB specimens, respectively, in MPa; Pmax is the peak load at failure, recorded in kN but substituted in N; all dimensions (h_1, h_2, L, b, D, t) are in mm. $\sigma_{\max}$ is the nominal tensile stress at failure of the SCB specimen, not the crack-tip stress; the coefficient 4.263 in Equation (3) is the elastic geometric factor for the SCB geometry with a support spacing of $0.8D$, taken from Hofman et al. [33], who determined it by elastic finite-element calibration. h_1 is the height of the IDT cylinder; h_2 and b are the height and width of the BBT mid-span cross-section; L is the BBT span; and D and t are the diameter and thickness of the semicircular specimen.

For all three tests, the fracture work was obtained from the load–displacement curve under a common recording convention. The load and crosshead (loading-head) displacement were recorded directly by the SANS machine without a separate deflection transducer, and the work was computed by integrating the load against this displacement; no system-compliance correction was applied. Because all specimens of a given geometry were tested on the same machine and setup, the machine compliance adds the same load-dependent displacement term to every specimen, introducing a common systematic bias that does not change the within-geometry relative rankings; it does, however, affect the absolute energy values, which should therefore be interpreted on a comparative rather than an absolute basis. The integral was taken to the end of the recorded curve, i.e., until the residual load had fallen to approximately 100 N or the specimen was completely fractured; for the brittle specimens at −10 °C the curve ended abruptly at failure, and the integral was taken to that point.

3. Results and Analysis

3.1. Comparison of Low-Temperature Fracture Test Methods for Asphalt Mixtures

3.1.1. Analysis of Fracture Process and Failure Characteristics

Generally, a steep drop immediately after the curve reaches the peak load, with an abrupt loss of load-bearing capacity, is classified as brittle fracture, whereas a complete

descending branch with continued load-bearing capacity indicates ductile fracture. The fracture mode can be determined from the shape of the load–displacement curve, as shown in Figure 5. It can be seen that all three mixtures in the BBT and SCB tests, as well as the base and SBS-modified asphalt mixtures in the IDT test, exhibit brittle fracture. Only the rubber-modified asphalt mixture in the IDT test shows a complete curve with a certain load-bearing capacity after the peak, indicating ductile failure. The comparison reveals contradictory fracture modes for the rubber-modified asphalt mixture across the three methods, initially exposing the limitation of the IDT test in evaluating its low-temperature performance.

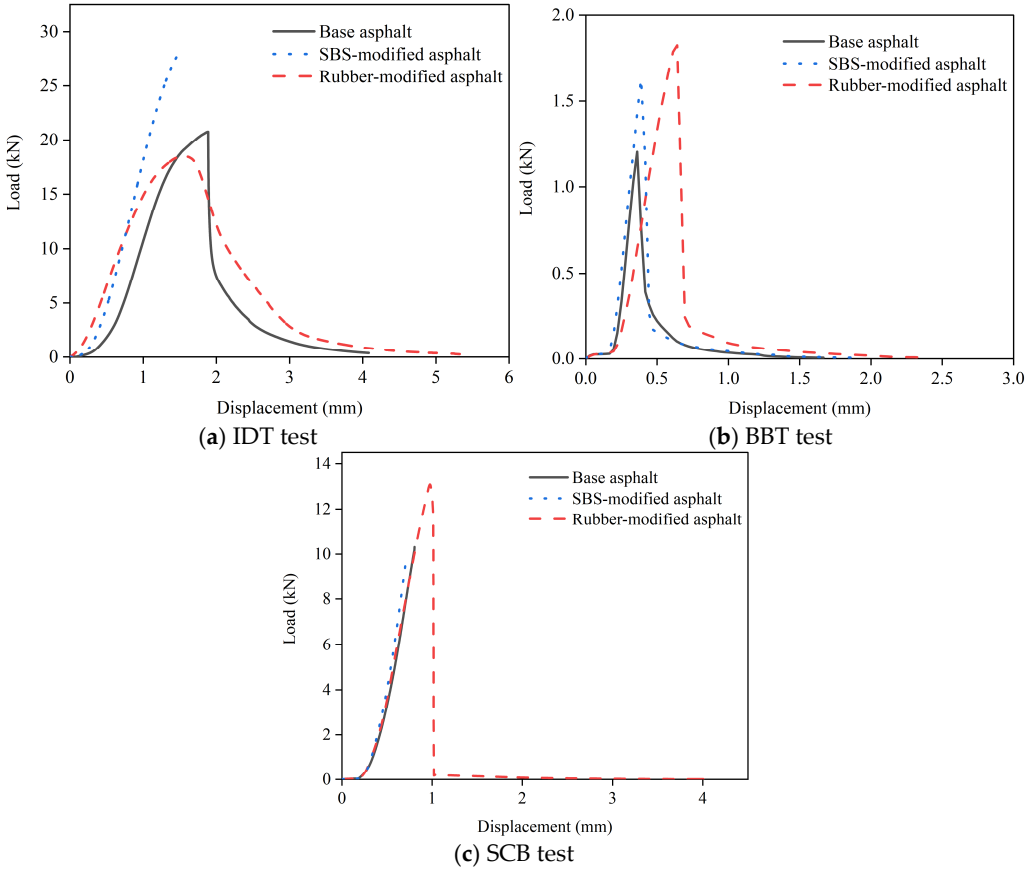
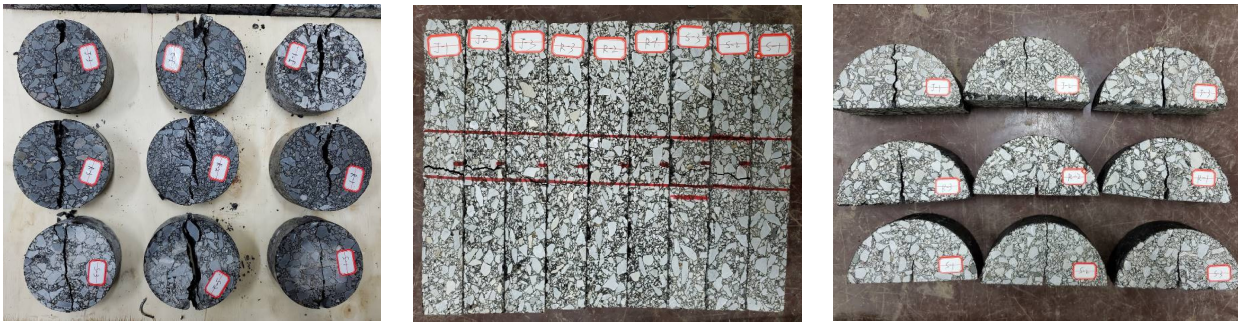


Figure 5. Load–displacement curves of the three tests.

In addition to the fracture process reflected by the load–displacement curves, the final failure morphology of the specimens also intuitively reflects the stress state of each test method. The failure modes of the failed specimens from the three methods are shown in Figure 6. In the IDT test, although the failure path propagates along the loading direction, obvious plastic deformation occurs beneath the loading strips, and a wedge-shaped body forms and crushes at the contact area under the combined action of compressive and shear stresses, indicating that the specimen is not in an ideal tensile state. In the BBT test, there is no obvious plastic deformation, but cracks mostly initiate from weak points at the bottom rather than at mid-span, with some exceeding the 0.1-span region from mid-span, indicating weak regularity. In the SCB test, roller loading is used with no obvious plastic deformation; cracks initiate from the notch tip and follow a regular, repeatable path along the binder before penetrating the specimen, giving the most reproducible failure mode and the geometry closest to ideal mode I (opening-mode) fracture. Here, a regular, repeatable crack path describes the controllability of the crack initiation location and propagation direction (a geometric/Mode-I feature that supports repeatability) and is distinct from

stable crack propagation, which denotes a post-peak ductile process. At −10 °C, the BBT and SCB specimens still failed in a brittle manner with a sudden post-peak load drop (Figure 5); the regular path therefore indicates good repeatability and a well-defined Mode-I geometry rather than stable crack growth.



(**a**) IDT test (**b**) BBT test (**c**) SCB test

Figure 6. Failure morphologies of specimens from the three tests.

The above qualitative observations were based on the load–displacement curve shapes and specimen failure morphologies. In the following, the three methods are further compared using quantitative indices such as peak load, tensile strength, and fracture work.

3.1.2. Comparison of Peak Load and Tensile Strength

The peak failure loads obtained from the three low-temperature fracture test methods are shown in Figure 7. The test results indicate that, for the same asphalt mixture, the peak failure loads obtained by different test methods follow the order BBT < SCB < IDT. However, the rankings differ for different asphalt mixtures using the same test method: in both the BBT and SCB tests, the peak failure loads follow rubber-modified > SBS-modified > base asphalt mixture, indicating that the rubber-modified asphalt mixture has the best low-temperature cracking resistance; in contrast, the IDT test yields the order SBS-modified > base > rubber-modified asphalt mixture, which contradicts the pattern obtained from the other two tests. This is because the IDT test uses a loading rate of 1 mm/min, at which the rubber-modified asphalt mixture exhibits viscoelastic characteristics with lower material stiffness, resulting in a lower peak failure load.

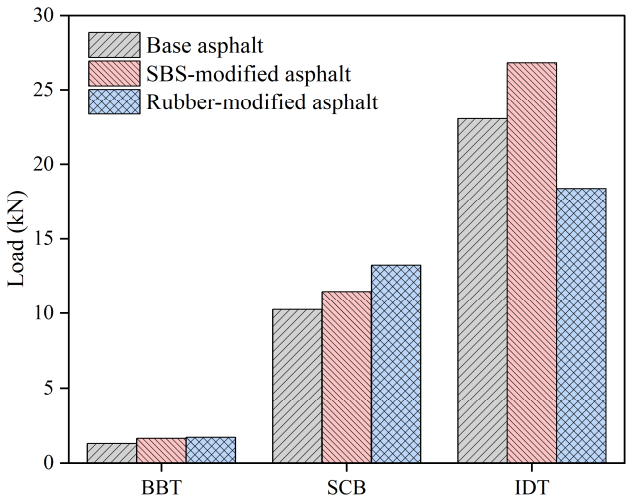


Figure 7. Peak failure loads of different asphalt mixtures.

The tensile strengths calculated from the peak failure loads are presented in Table 5. Because the three methods differ in specimen dimensions and loading mode, the absolute magnitude order of strength (BBT > SCB > IDT) does not directly reflect the performance of the mixtures; the key lies in the ability of each method to discriminate among the three asphalt mixtures. Although the IDT test measures a larger load, the converted strength is the lowest, and its discrimination pattern for the rubber-modified asphalt mixture is anomalous, indicating weak index sensitivity. In the BBT test, the strength values of the SBS-modified and rubber-modified asphalt mixtures are relatively close, making it difficult to distinguish between them. In the SCB test, the strength values show clear discrimination, distinctly reflecting the quality order of the three mixtures, consistent with the BBR test results.

Table 5. Tensile strength of the three test methods at −10 °C (mean ± SD, $n = 3$; CV in parentheses).

Asphalt Mixture Type	IDT Strength/MPa	BBT Strength/MPa	SCB Strength/MPa
Base asphalt mixture	3.62 ± 0.38 (10.5%)	10.54 ± 1.18 (11.2%)	5.83 ± 0.18 (3.0%)
SBS-modified asphalt mixture	4.22 ± 0.43 (10.3%)	13.26 ± 0.82 (6.2%)	6.52 ± 0.62 (9.5%)
Rubber-modified asphalt mixture	2.89 ± 0.25 (8.8%)	13.77 ± 1.33 (9.7%)	7.52 ± 0.39 (5.2%)

To assess repeatability and discrimination rather than to establish a statistical superiority ranking between methods, the coefficient of variation (CV) was used to measure repeatability, and one-way analysis of variance (ANOVA) was performed at $\alpha = 0.05$ to test whether the tensile strength differed significantly among the three mixtures, with the effect size η^2 (the proportion of variance explained by mixture type) quantifying discrimination. The CV varies with mixture type: for the SBS-modified mixture, it is higher in the SCB test (9.5%) than in the BBT test (6.2%). Nevertheless, the mean within-mixture CV is the lowest for the SCB (5.9%, versus 9.0% for the BBT and 9.9% for the IDT), so the repeatability advantage of the SCB is a general tendency within the dataset examined rather than a guarantee for every mixture. The three mixtures differ significantly relative to their within-mixture scatter for every method (IDT: $F = 9.99$, $p = 0.0123$, $\eta^2 = 0.77$; BBT: $F = 7.03$, $p = 0.0268$, $\eta^2 = 0.70$; SCB: $F = 11.88$, $p = 0.0082$, $\eta^2 = 0.80$); F and η^2 quantify the between-mixture difference relative to the within-mixture scatter within each method, i.e., the discrimination ability of each method among the three mixtures; the SCB test shows the largest F and η^2, indicating the clearest between-mixture discrimination within this method. However, because these statistics describe differences among mixtures within each method rather than differences between methods, they do not, by themselves, establish that one method is statistically superior to another. With only three specimens per condition, these results are indicative rather than conclusive. It should be noted that the tensile strength is linearly derived from the peak load, so the same CV and significance results apply to the peak load; the fracture work, an absolute energy quantity dependent on specimen geometry (Section 3.1.3), is not used for this scatter-based comparison.

3.1.3. Comparison of Fracture Work

The fracture work of the three asphalt mixtures under different test methods is compared in Figure 8.

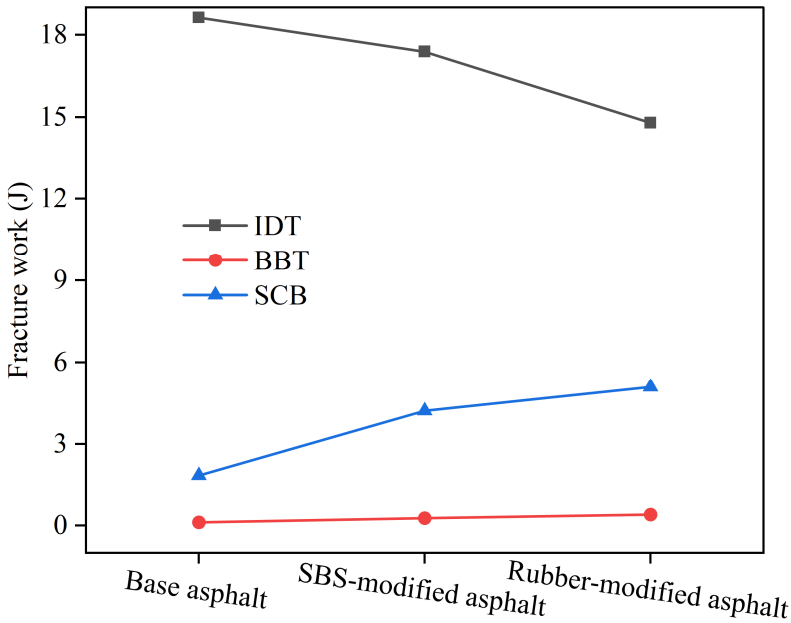


Figure 8. Fracture work of specimens from the three asphalt mixtures.

As fracture work is an absolute energy quantity that depends on specimen dimensions and loading configuration, its absolute values cannot be compared directly across the three methods; as for tensile strength, the methods are evaluated by the relative ranking of the three mixtures within each method and by their discrimination ability. The results show that, for each asphalt mixture, the absolute fracture work still follows the order IDT > SCB > BBT, which is governed mainly by specimen geometry and is not used as a direct basis for method comparison. However, for different asphalt mixtures, the fracture work in the IDT test follows base > SBS-modified > rubber-modified asphalt mixture, which is clearly inconsistent with the facts—the cracking resistance of the SBS-modified asphalt mixture should be superior to that of the base asphalt mixture. In contrast, the fracture work in both the SCB and BBT tests follows rubber-modified > SBS-modified > base asphalt mixture, consistent with the low-temperature performance pattern revealed by the asphalt BBR test. This indicates that, under the present procedures, the IDT test has considerable limitations when fracture work is used as the evaluation index.

In terms of numerical characteristics, the fracture work in the BBT test is less than 0.5 J for all mixtures, which is relatively small; the fracture work in the SCB test is greater than 1 J for all mixtures, with clear discrimination among different mixtures and stable parallel test data.

3.1.4. Comprehensive Comparison of Test Methods

Combining the qualitative observations of fracture process and failure characteristics with the three quantitative indices of peak load, tensile strength, and fracture work, two points can be summarized: (1) Under the present procedures, the IDT test exhibits anomalous fracture mode discrimination and crushing failure beneath the loading strips, and its peak load and fracture work give contradictory quality rankings for the three asphalt mixtures, indicating limited evaluation reliability for the tested mixtures and indices. (2) In both the BBT and SCB tests, the crack path is relatively regular and reproducible, with no obvious crushing failure, and the three quantitative indices give consistent quality rankings—rubber-modified > SBS-modified > base asphalt mixture. This ranking is consistent with the low-temperature performance of the raw binders indicated by the BBR test,

providing corroborating evidence from the binder level. The regular crack paths and the consistent rankings indicate good reliability and repeatability.

Between the BBT and SCB methods, the SCB test shows clearer discrimination and stronger sensitivity for the three mixtures across all three indices. Moreover, SCB specimens can be prepared from field core samples, facilitating on-site pavement quality inspection, whereas BBT specimens are difficult to form and unsuitable for field sampling. Considering both qualitative phenomena and quantitative indices, among the three methods under the present procedures, the SCB test shows the most favorable reliability, repeatability, and sensitivity for the mixtures examined, and is therefore adopted as the method for the subsequent parameter study rather than as a universally validated optimum.

3.2. Influence of Test Parameters on Cracking Evaluation Indices Based on the SCB Test

Based on the above comparison results, the SCB test showed the best reliability and discrimination among the three methods under the −10 °C comparison and was selected for the following parameter study. The purpose of this stage was to determine a suitable routine test condition for the selected SCB method by examining the effects of asphalt type, temperature (5–25 °C), loading rate and notch depth on the cracking evaluation indices; the following two sets of tests were conducted: first, using 70# base and SBS-modified asphalt mixtures, SCB tests were performed at 5 °C, 15 °C, and 25 °C under a loading rate of 5 mm/min and a notch depth of 10 mm to compare the index responses of different asphalt types at various temperatures; second, the SBS-modified asphalt mixture—which is the most widely used polymer-modified asphalt type in high-grade asphalt pavements and is therefore a representative material—was used in a three-factor three-level experimental scheme, selecting temperature (5 °C, 15 °C, and 25 °C), loading rate (0.5 mm/min, 5 mm/min, and 50 mm/min), and notch depth (10 mm, 15 mm, and 20 mm) as the three factors, with three parallel specimens per group, to systematically analyze the influence of each factor on the cracking evaluation indices. The same SANS universal testing machine and data acquisition setting (32 Hz) as in Section 2.2 were used for all SCB tests in this section.

Three cracking evaluation indices were adopted in this section: fracture toughness J_{IC}, fracture toughness K_{IC}, and fracture energy G_f. The calculation methods for each index are as follows:

(1) Fracture energy G_f. Fracture energy is the ratio of fracture work W_f to the ligament area A_{lig}, calculated using Equation (4):

$$G_f = \frac{W_f}{A_{lig}} \tag{4}$$

where G_f is the fracture energy (J/m^2); W_f is the fracture work (J); and A_{lig} is the ligament area (m^2), given by $A_{lig} = (r - a) \cdot t$, where r is the specimen radius (m), a is the notch depth (m), and t is the specimen thickness (m).

(2) Fracture toughness K_{IC}. K_{IC} is an important parameter describing the fracture behavior of elastic materials, calculated using Equation (5):

$$K_{IC} = \sigma_{\max} \cdot f\left(\frac{a}{W}\right) \tag{5}$$

where K_{IC} is the fracture toughness ($N/mm^{3/2}$); σ is the failure strength (N/mm^2); and f is the specimen geometry factor ($mm^{1/2}$), determined from the notch depth a and specimen height W (both in mm).

When $9 < a < 11$ mm and $70 < W < 75$ mm, $f = 5.956$. For other values of a and W, f is obtained from Equation (6):

$$f(\frac{a}{W}) = -4.9965 + 155.58(\frac{a}{W}) - 799.94(\frac{a}{W})^2 + 2141.9(\frac{a}{W})^3 - 2709.1(\frac{a}{W})^4 + 1398.6(\frac{a}{W})^5 \quad (6)$$

(3) Fracture toughness J_{IC}. Based on J-integral theory, the fracture work W_f is obtained from the area under the load–displacement curve, and dividing by the specimen thickness B gives the fracture energy per unit thickness W_f/B. The J-integral characterizes fracture toughness from the perspective of energy release rate, and its critical value J_{IC} equals the rate at which the fracture energy per unit thickness decreases with increasing notch depth (i.e., crack length). To this end, semicircular specimens with notch depths of 10 mm, 15 mm, and 20 mm were tested, and the fracture energy per unit thickness at each notch depth was calculated. A linear relationship between fracture energy per unit thickness and notch depth was established, and the negative value of the slope of the fitted line is the J_{IC} value. The J-integral avoids analysis of the complex stress–strain field at the crack tip, has a clear physical meaning, and is suitable for evaluating the cracking resistance of viscoelastoplastic materials such as asphalt mixtures [34].

3.2.1. Comparison of Cracking Evaluation Indices for Different Asphalt Mixtures

The variations of K_{IC} and G_f with temperature for the two asphalt mixtures are shown in Figure 9. At the same temperature, both index values of the SBS-modified asphalt mixture are greater than those of the base asphalt mixture, indicating that both K_{IC} and G_f can distinguish the difference between the two asphalts. The two indices show different temperature responses: K_{IC} decreases monotonically with increasing temperature, with the most significant discrimination between the two mixtures at 25 °C; as an energy-based index, G_f first increases and then decreases with increasing temperature, reaching a peak at 15 °C, and shows good discrimination at both 5 °C and 25 °C. It should be noted that J_{IC} is determined from specimens with three notch depths, so it is analyzed in the parameter study of Section 3.2.2 rather than in this single-notch comparison.

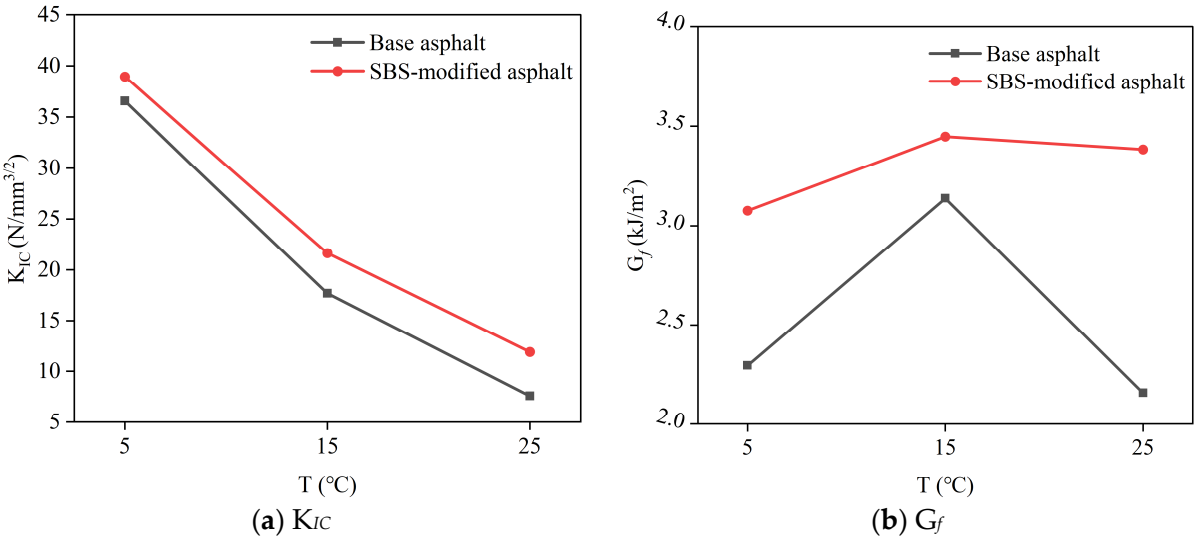


Figure 9. Variation in cracking evaluation indices with temperature for different asphalt mixtures.

3.2.2. Analysis of Influencing Factors on Fracture Toughness J_{IC}

Using the SBS-modified asphalt mixture as the object, the influencing factors on J_{IC} were further analyzed. It should be noted that J_{IC} is obtained by linear fitting of the fracture energy per unit thickness at notch depths of 10 mm, 15 mm, and 20 mm; the notch depth is an inherent variable in its calculation rather than an external factor under investigation.

Therefore, this section focuses on the effects of temperature and loading rate on J_{IC}. The influence of loading rate on the fracture energy per unit thickness is shown in Figure 10. At 5 °C, 15 °C, and 25 °C, the fracture energy per unit thickness decreases with increasing notch depth and shows a good linear correlation with notch depth (the linear correlation coefficients of all nine fitted lines are greater than 0.877). Because each J_{IC} is derived from only three notch-depth values, the regression remains sensitive to the scatter of any single point, so the high R^2 alone does not establish robustness; the J_{IC} values are therefore used mainly for relative comparison under the same procedures rather than as precise absolute values. At 5 °C, J_{IC} is maximum at a loading rate of 5 mm/min (10.400 kJ/m^2) and minimum at 50 mm/min (3.337 kJ/m^2). This is because at low temperature and high loading rate, the specimen is stiffer and behaves in an elastic, brittle manner: it reaches a larger peak load while the post-peak stage is almost absent, so the total fracture energy, including the post-peak crack-propagation energy, is small. At 15 °C, J_{IC} is lowest at 5 mm/min (5.083 kJ/m^2) and highest at 50 mm/min (6.887 kJ/m^2); at 25 °C, J_{IC} is similarly high at 5 and 50 mm/min (about 10.8 kJ/m^2) and much lower at 0.5 mm/min (5.920 kJ/m^2). The dependence of J_{IC} on loading rate is therefore non-monotonic and temperature-dependent, and the combination of 5 °C and 50 mm/min gives an exceptionally low J_{IC} owing to brittle fracture.

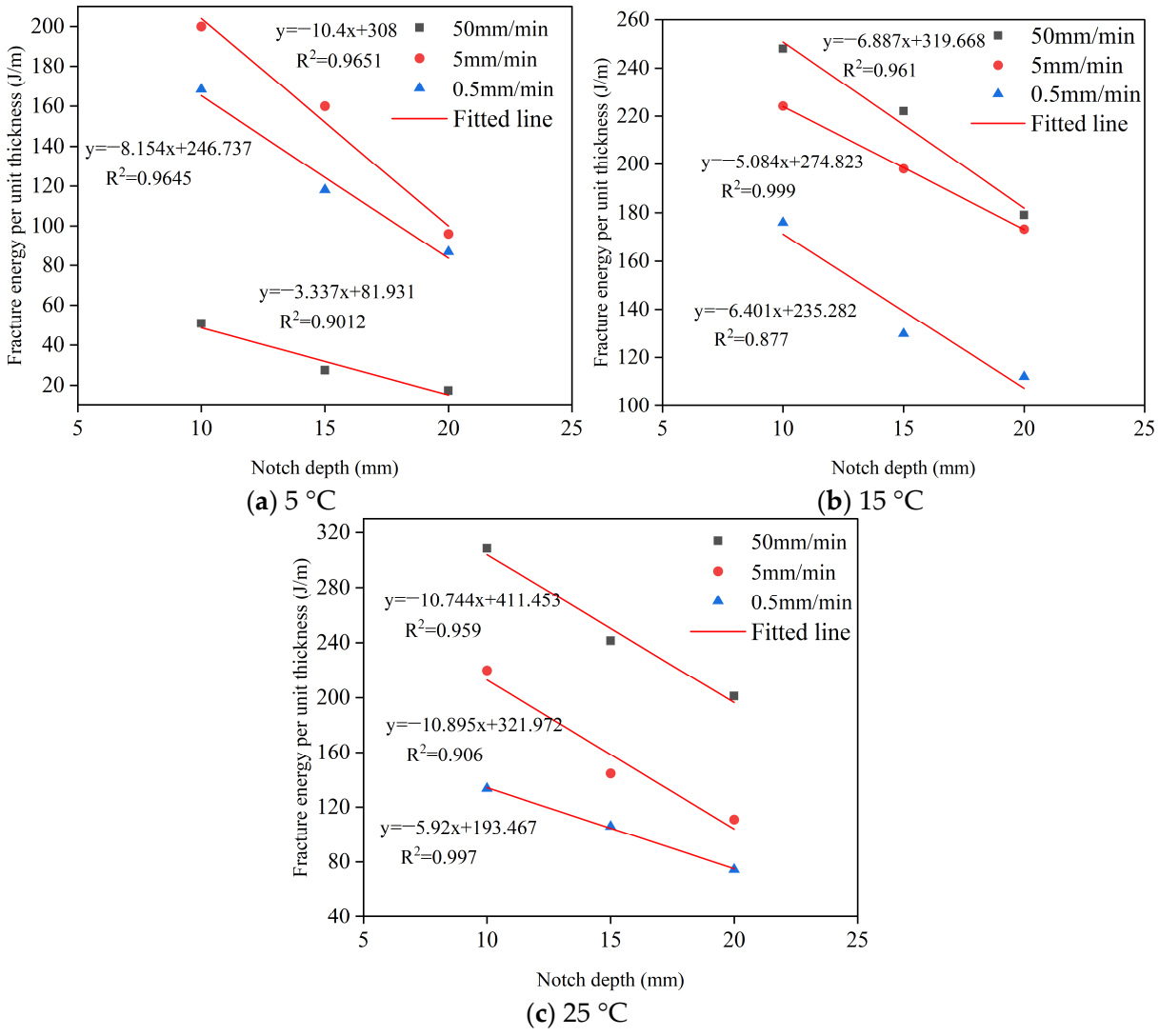


Figure 10. Influence of loading rate on fracture energy per unit thickness at different temperatures.

The influence of temperature on the fracture energy per unit thickness is shown in Figure 11. At a loading rate of 50 mm/min, J_{IC} increases monotonically with temperature (from 3.337 to 10.744 kJ/m^2), whereas at 0.5 mm/min it decreases monotonically (from 8.154 to 5.920 kJ/m^2); at 5 mm/min, however, J_{IC} varies non-monotonically, reaching a minimum at 15 °C (5.083 kJ/m^2). The reversal of the temperature effect with loading rate indicates an interaction between temperature and loading rate, and J_{IC} is sensitive to the test conditions, so comparisons must be made under fixed conditions. In particular, the combination of 5 °C and 50 mm/min leads to anomalously brittle fracture with an exceptionally low J_{IC}. Given the limited number of replicates, this interaction is interpreted qualitatively rather than statistically quantified.

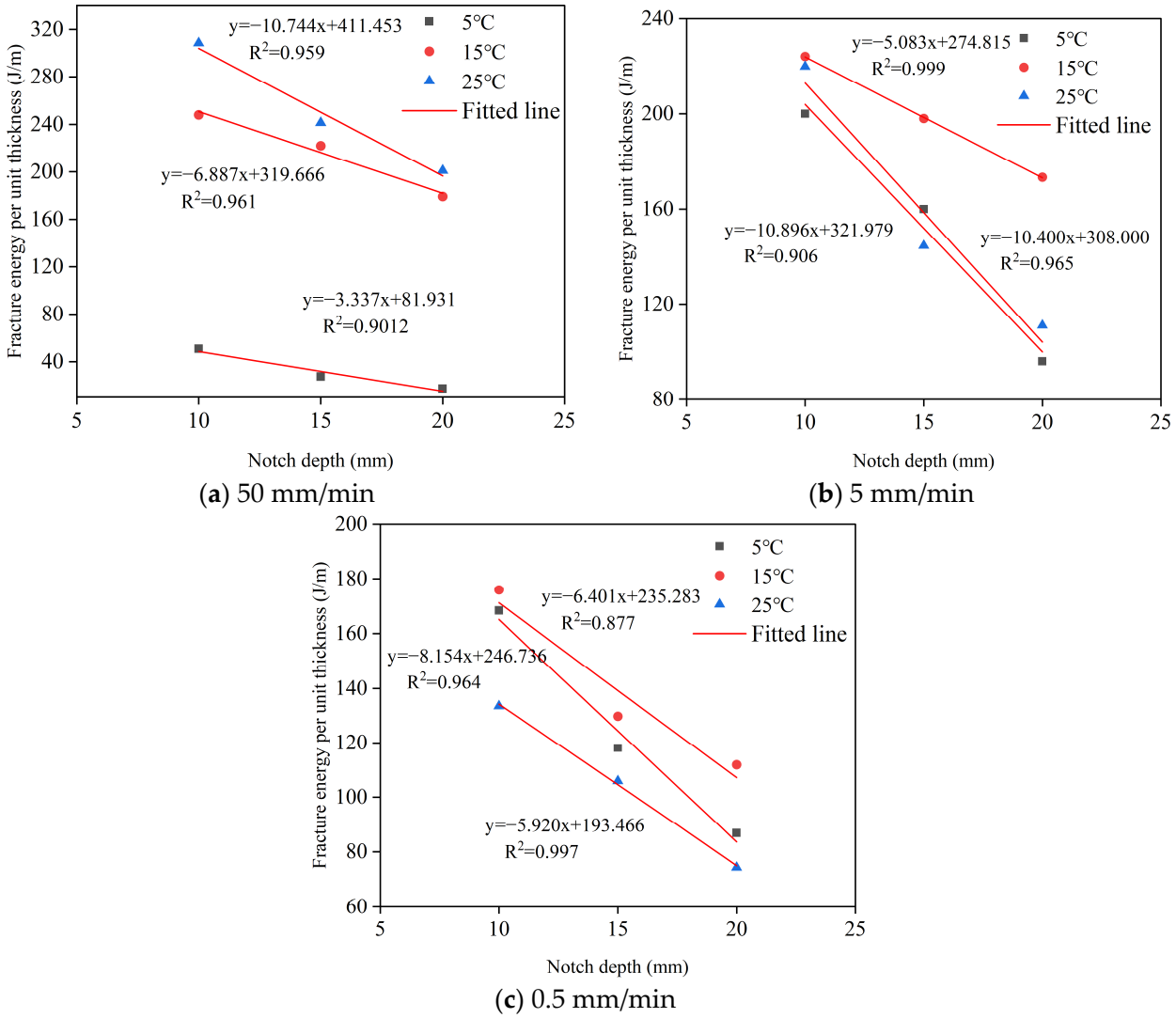


Figure 11. Influence of temperature on fracture energy per unit thickness at different loading rates.

3.2.3. Analysis of Influencing Factors on Fracture Toughness K_{IC}

K_{IC} is simultaneously affected by temperature, loading rate, and notch depth. To clarify the behavior of the three factors, the coupled influence of two factors was examined separately while fixing the third. The combined influence of loading rate and notch depth is shown in Figure 12. At all three temperatures (5 °C, 15 °C, and 25 °C), K_{IC} decreases with decreasing loading rate and increasing notch depth. K_{IC} reaches its maximum at a notch depth of 10 mm and a loading rate of 50 mm/min and its minimum at a notch depth of

20 mm and a loading rate of 0.5 mm/min. Thus, the main effects of loading rate and notch depth on K_{IC} are in the same direction—both reduce K_{IC}—but their degrees of influence vary with temperature. At 5 °C, the decrease in K_{IC} when the loading rate drops from 5 mm/min to 0.5 mm/min is significantly greater than that from 50 mm/min to 5 mm/min, while the variation with notch depth from 10 mm to 20 mm is relatively gentle, indicating that the influence of loading rate is greater than that of notch depth at this temperature. When the temperature rises to 15 °C and 25 °C, the decrease in K_{IC} caused by loading rate variation is significantly smaller than at 5 °C, i.e., the influence of loading rate weakens with increasing temperature.

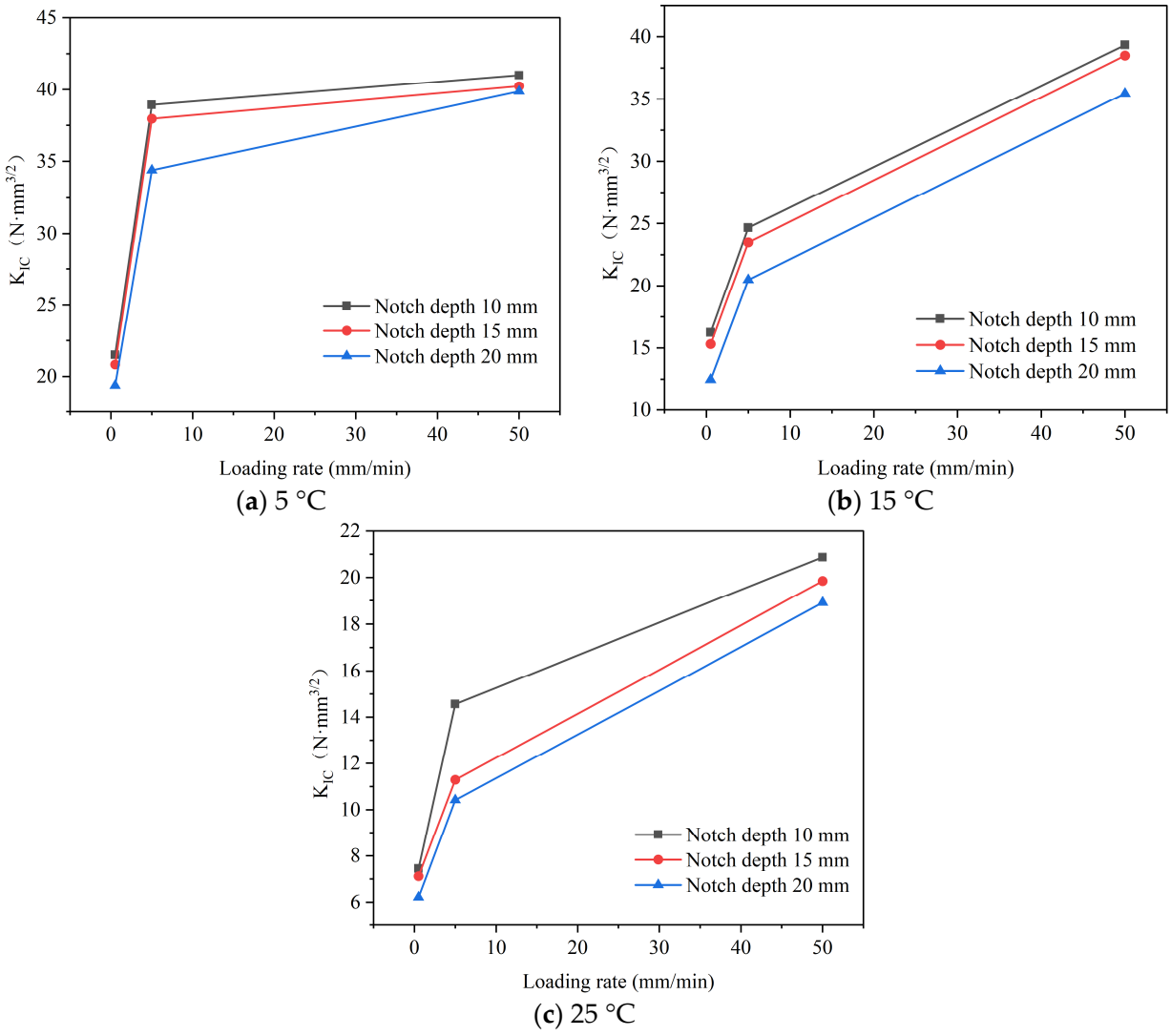


Figure 12. Influence of loading rate and notch depth on K_{IC}.

The combined influence of loading rate and temperature is shown in Figure 13. At different notch depths, K_{IC} decreases with decreasing loading rate and increasing temperature. The maximum K_{IC} is obtained at 50 mm/min and 5 °C, and the minimum at 0.5 mm/min and 25 °C. The variation trends of K_{IC} are similar for all three notch depths, indicating that loading rate and temperature have significant effects on K_{IC}, and these two parameters must be specified in the test.

Regarding the combined influence of notch depth and temperature (Figure 14), K_{IC} decreases with increasing notch depth and temperature. At a loading rate of 50 mm/min, K_{IC} exhibits a piecewise pattern of initially gentle variation followed by a steep drop with

temperature; this is because at low temperature and high loading rate, the specimen is dominated by elastic deformation, whereas at 25 °C it is dominated by elastoplastic deformation. At lower loading rates, K_{IC} decreases approximately linearly with temperature. Comprehensive comparison shows that K_{IC} drops sharply in the 15–25 °C range, while varying relatively gently with notch depth, indicating that the influence of temperature on K_{IC} is far greater than that of notch depth.

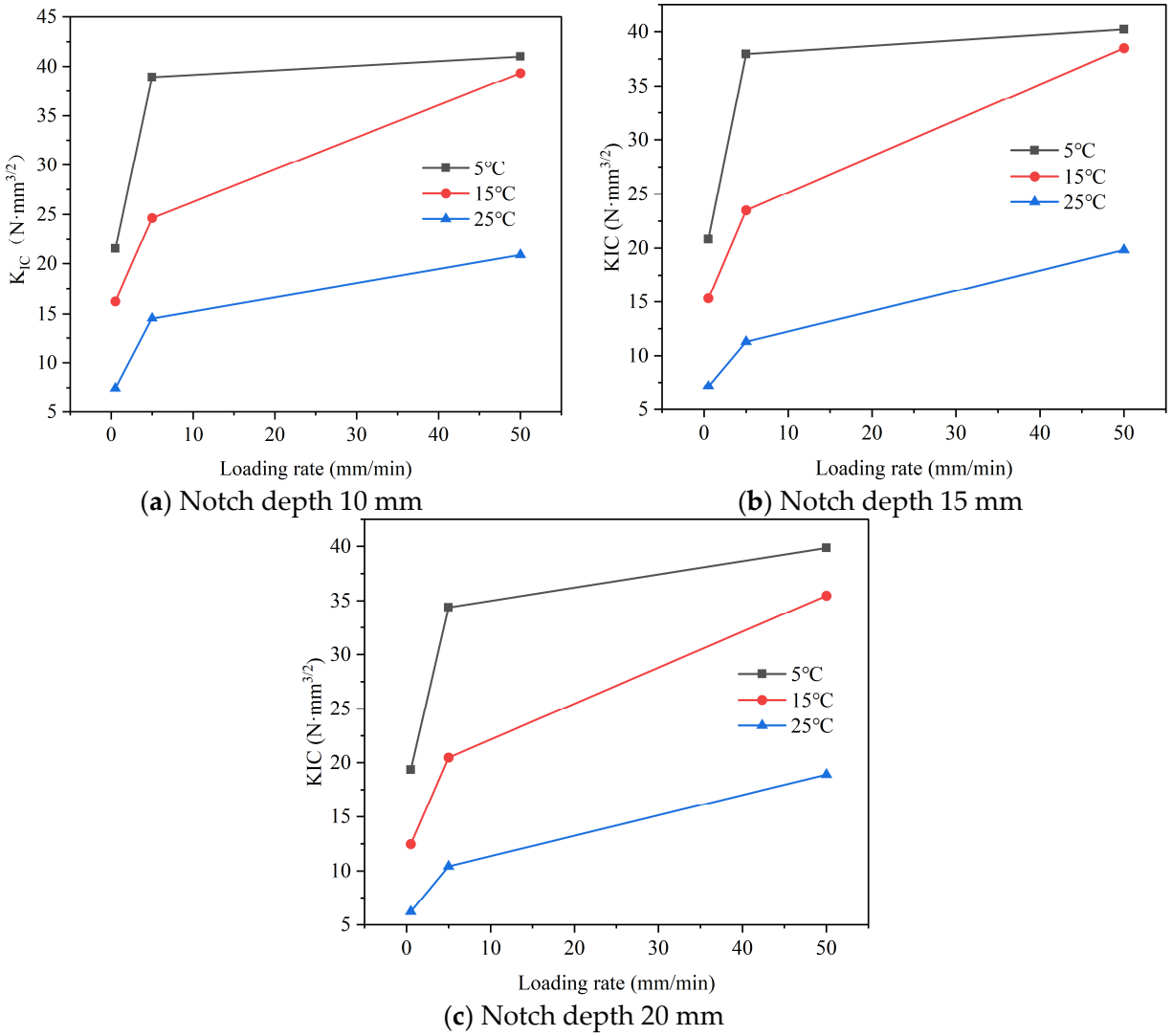


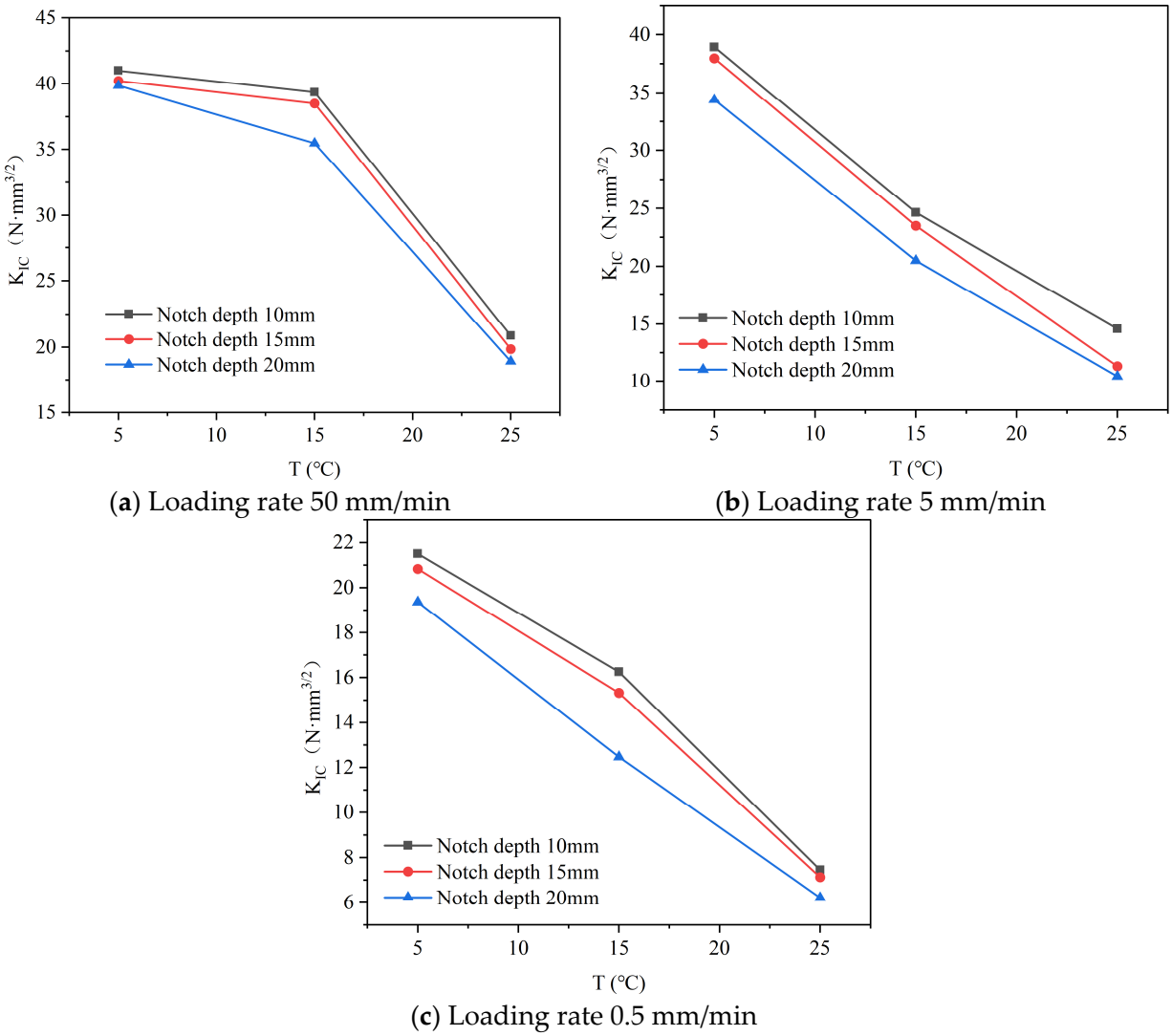
Figure 13. Influence of loading rate and temperature on K_{IC}.

In summary, at ambient temperature, K_{IC} is not a constant material parameter but varies with temperature, loading rate, and notch depth. This is because at ambient temperature, asphalt mixtures are in a viscoelastoplastic state, and the plastic zone at the crack tip is relatively large, deviating from the small-scale yielding assumption of linear elastic fracture mechanics; K_{IC} is therefore no longer a purely intrinsic material value. Consequently, when using K_{IC} for evaluation, the test temperature, loading rate, and notch depth must be fixed, and results under different conditions should not be directly compared.

3.2.4. Analysis of Influencing Factors on Fracture Energy G_f

G_f is also jointly affected by temperature, loading rate, and notch depth. Below, the coupled influence of two factors is examined separately while fixing the third. The combined influence of loading rate and notch depth is shown in Figure 15, and its behavior falls into two

cases depending on temperature. At 15 °C and 25 °C (ductile fracture state), G_f decreases with increasing notch depth and increases with increasing loading rate, so its maximum occurs at the combination of 50 mm/min and a notch depth of 10 mm. At 5 °C, G_f still decreases with increasing notch depth but first increases and then decreases with increasing loading rate, with the maximum at 5 mm/min and the minimum at 50 mm/min, contrary to the monotonically increasing pattern with loading rate at 15 °C and 25 °C. This anomaly is due to brittle fracture at 5 °C and 50 mm/min: after the load reaches its peak, the specimen fails immediately without a ductile fracture stage, resulting in smaller fracture work, as shown by the load–displacement curve in Figure 16. Further comparison of the influence magnitudes of each factor shows that at 15 °C and 25 °C, the variation in G_f caused by changing the loading rate at a fixed notch depth is relatively large, whereas the variation in G_f when changing the notch depth at a fixed loading rate is relatively gentle, indicating that the influence of loading rate on G_f is significantly greater than that of notch depth in this temperature range.



(**a**) Loading rate 50 mm/min (**b**) Loading rate 5 mm/min

(**c**) Loading rate 0.5 mm/min

Figure 14. Influence of notch depth and temperature on K_{IC}.

The combined influence of loading rate and temperature is shown in Figure 17. At 5 °C, G_f follows the order 5 mm/min > 0.5 mm/min > 50 mm/min; at 15 °C and 25 °C, G_f increases with increasing loading rate. At loading rates of 5 mm/min and 0.5 mm/min, G_f first increases and then decreases with increasing temperature, reaching a peak at 15 °C. This

is because when the temperature rises from 5 °C to 15 °C, the material transitions from elastic-dominated to elastoplastic-dominated deformation; although the peak load decreases, the failure displacement increases significantly, causing the fracture energy to increase. When the temperature rises from 15 °C to 25 °C, the material stiffness further decreases, and the fracture energy declines. At a loading rate of 50 mm/min, however, G_f increases continuously with temperature without a peak at 15 °C, indicating an interaction between loading rate and temperature: a high loading rate changes the temperature-response pattern of G_f.

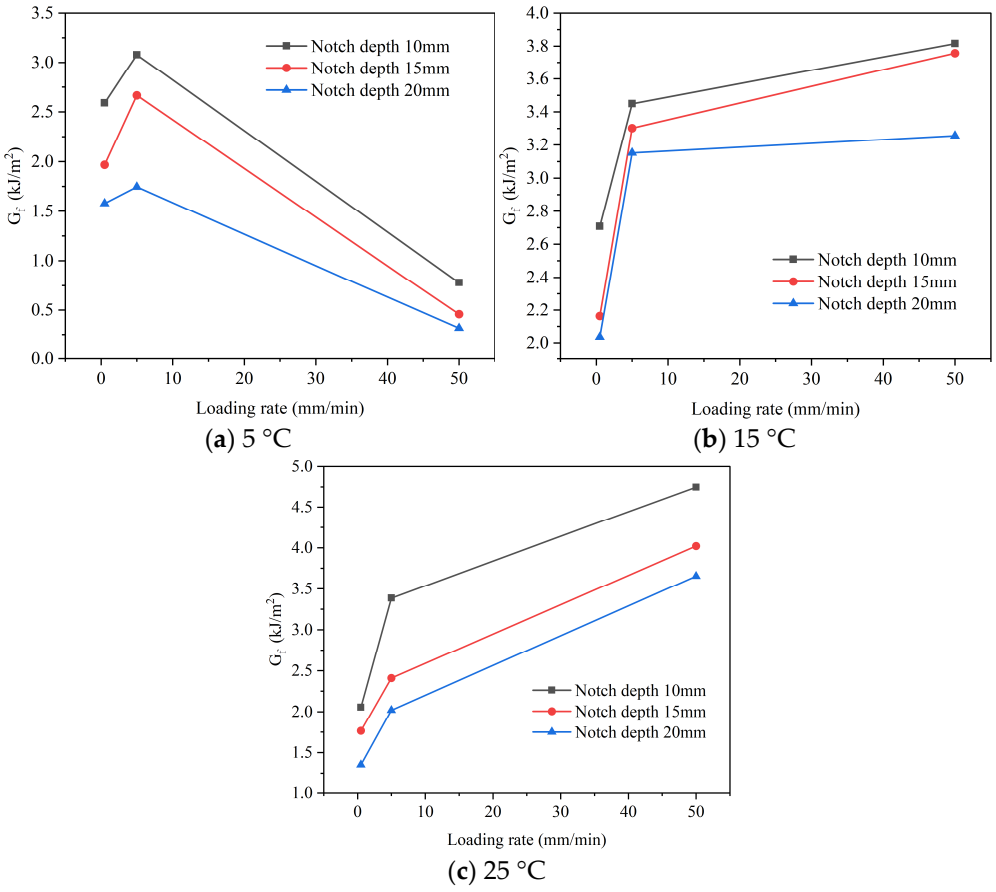


Figure 15. Influence of loading rate and notch depth on G_f.

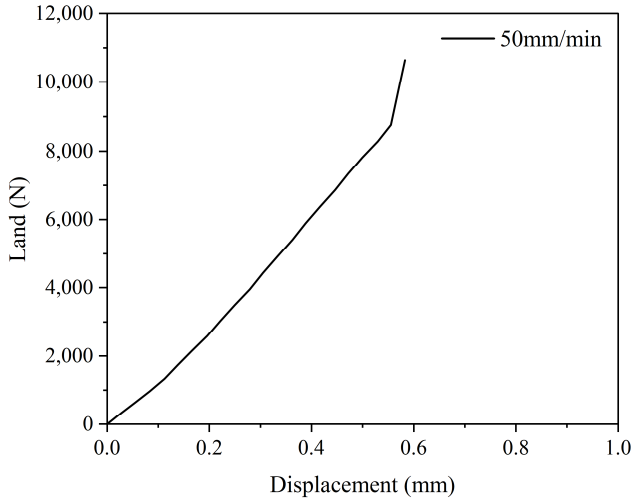


Figure 16. Load–displacement curve at 5 °C and a loading rate of 50 mm/min.

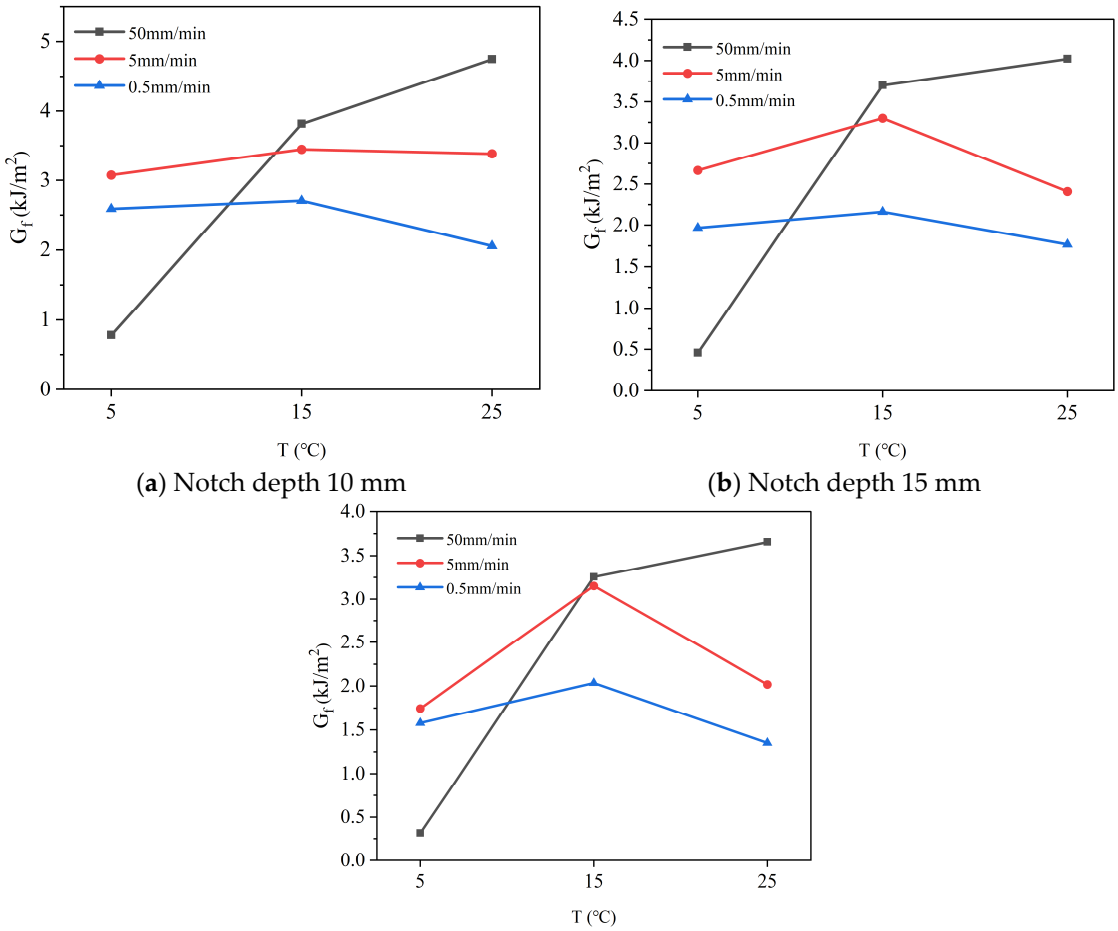


Figure 17. Influence of loading rate and temperature on G_f.

In addition, the internal failure characteristics of specimens at 15 °C under different loading rates were observed, as shown in Figure 18. It was found that as the loading rate decreases, cracks increasingly propagate along the binder and aggregate–binder interface rather than through the aggregates, which may indicate that at a slower rate the fracture process zone develops more fully and the crack propagates in a more stable and observable manner [35]. Considering that excessively low loading rates unduly prolong the test, a loading rate no greater than 5 mm/min but not excessively small is adopted.

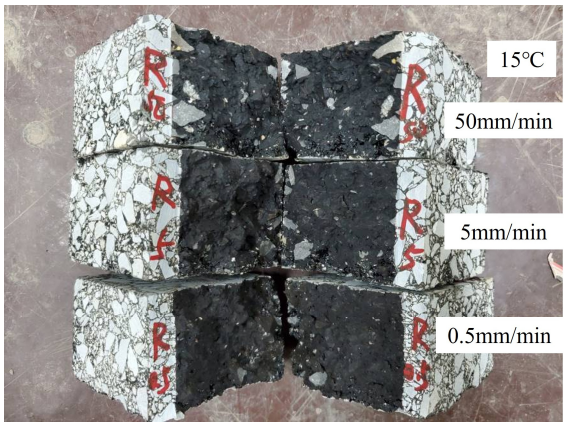
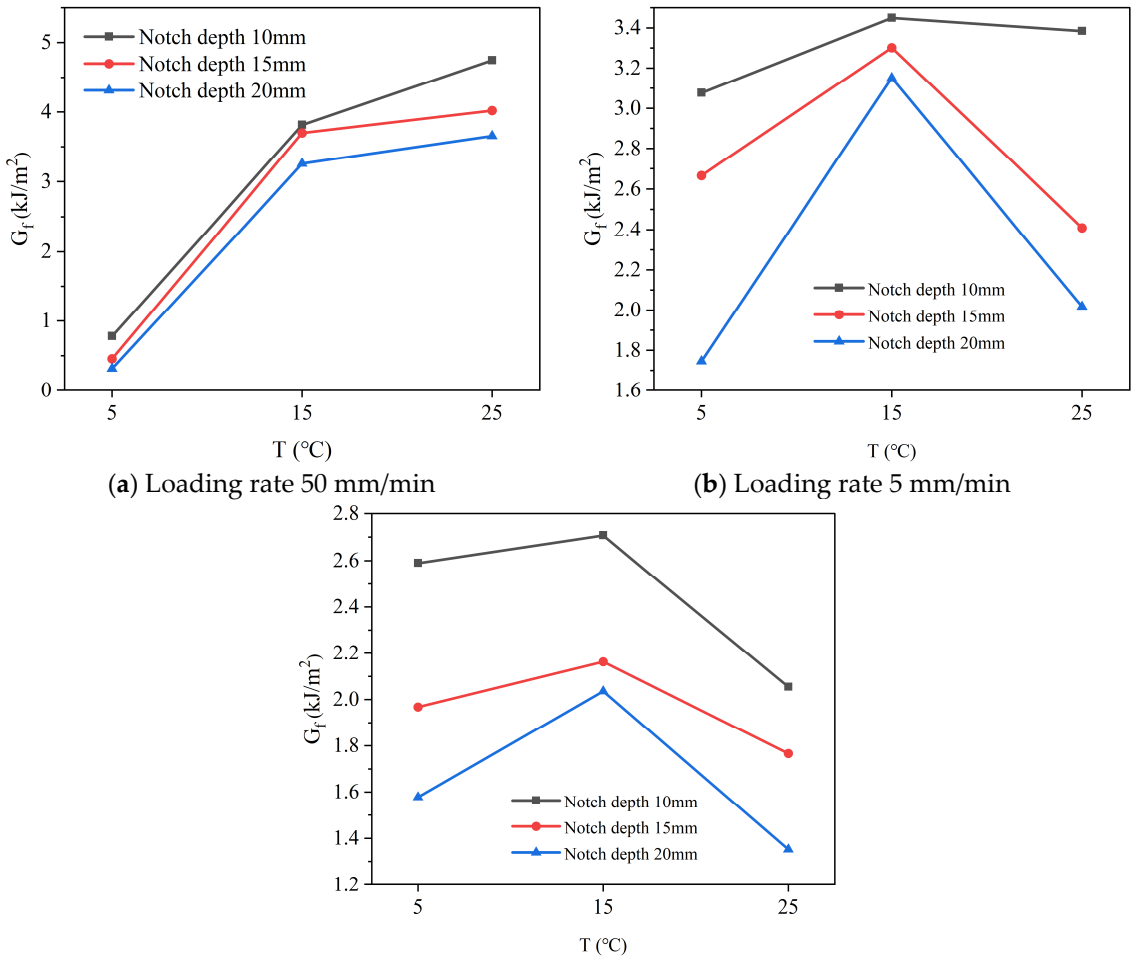


Figure 18. Internal failure characteristics of semicircular specimens at different loading rates.

Further examining the influence of temperature and notch depth on G_f, as shown in Figure 19, the effect of notch depth is mainly reflected in the magnitude of G_f: at all loading rates and temperatures, G_f decreases with increasing notch depth. A possible interpretation is that the fracture work is dissipated not only on the new crack surface (in proportion to A_{lig}) but also in the fracture process zone (FPZ) ahead of the crack tip; as the notch deepens and the remaining ligament shortens, the FPZ may be increasingly constrained by the specimen boundaries and unable to fully develop, so W_f decreases more rapidly than A_{lig} [36]. Hence, even though $G_f = W_f/A_{lig}$ is normalized by A_{lig}, G_f still decreases with increasing notch depth, which can be regarded as a geometry (size) effect arising when the ligament length becomes comparable to the FPZ characteristic size. Note that the FPZ was not directly measured; this mechanism is therefore an interpretation of the experimental results rather than a demonstrated mechanism [35]. However, notch depth does not alter the variation pattern of G_f with temperature: at 5 mm/min and 0.5 mm/min, regardless of whether the notch depth is 10 mm, 15 mm, or 20 mm, G_f always peaks at 15 °C; at 50 mm/min, G_f always increases continuously with rising temperature. That is, notch depth only affects the absolute value of G_f and does not change the trend of its temperature response or the peak temperature point.



(**a**) Loading rate 50 mm/min

(**b**) Loading rate 5 mm/min

(**c**) Loading rate 0.5 mm/min

Figure 19. Influence of temperature and notch depth on G_f.

Based on the above results, the conditions of 25 °C, 5 mm/min, and a notch depth of 10–15 mm are proposed as a routine ambient-temperature condition for the SCB test rather than a low-temperature screening condition. The rationale is as follows: at the low

temperature of 5 °C, the material is relatively brittle and prone to brittle fracture, making it difficult to reflect the viscoelastoplastic fracture characteristics of asphalt mixtures; at the high loading rate of 50 mm/min, cracks tend to penetrate aggregates rather than propagate along the binder; although 0.5 mm/min allows an even more stable fracture, the test time is relatively long; an excessively deep notch (20 mm) may leave too short a ligament for the fracture process to fully develop, yielding a low G_f. Under the proposed conditions, the material is dominated by elastoplastic deformation, and cracks propagate stably along the binder, facilitating observation with moderate test efficiency.

It should be noted that the standardized SCB protocols serve different evaluation purposes: the 50 mm/min rate in the I-FIT (AASHTO TP124) [26] is designed for rapid flexibility-index screening, whereas the 5 mm/min rate in EN 12697-44 [25] is used for fracture-toughness (K_{IC}) determination. In this study, 5 mm/min is used to determine K_{IC}, with J_{IC} and G_f further derived under the same configuration, and this rate is consistent with the EN fracture-toughness test; the proposed conditions are therefore a complement to, rather than a replacement for, these standardized protocols.

4. Conclusions

Using three types of AC-13 asphalt mixtures, this study compared the IDT, BBT, and SCB methods at −10 °C and further examined the influence of test parameters on the fracture indices. The main conclusions are as follows:

(1) The IDT test exhibits anomalous fracture discrimination, crushing beneath the loading strips, and contradictory rankings between peak load and fracture work, indicating insufficient reliability under the present −10 °C procedures. Both the BBT and SCB tests show relatively regular and reproducible crack paths, along with consistent rankings across the three indices (rubber > SBS > base, agreeing with BBR results); however, the SCB test offers better discrimination and allows field core sampling, making it the preferred cracking resistance evaluation method among the three under these conditions.

(2) Under the SCB test, K_{IC} and G_f can distinguish different asphalt mixtures, with the index values of the SBS-modified asphalt mixture greater than those of the base asphalt mixture. K_{IC} decreases monotonically with increasing temperature, while G_f, as an energy-based index, first increases and then decreases with temperature and peaks at 15 °C. J_{IC} is strongly dependent on temperature and loading rate, and the three indices exhibit distinct responses to temperature and loading conditions and can complement one another.

(3) K_{IC} increases with increasing loading rate and decreases with increasing temperature and notch depth; the influence of temperature is far greater than that of notch depth, with a sharp drop in the 15–25 °C range. At ambient temperature, K_{IC} is not a constant because the material is in a viscoelastoplastic state and deviates from the small-scale yielding assumption of linear elastic fracture mechanics; therefore, the test temperature, loading rate, and notch depth must be fixed when using K_{IC}.

(4) G_f decreases with increasing notch depth; under ductile fracture, it increases with increasing loading rate, while at 5 °C and high loading rate, an anomalously low value occurs due to brittle fracture. There is an interaction between loading rate and temperature on Gf: at 50 mm/min the temperature response of Gf changes from a 15 °C-peak pattern to a monotonic increase, whereas at lower loading rates cracks tend to propagate along the binder and the aggregate–binder interface, allowing a more stable and fully developed fracture process.

(5) Considering the influence of all factors, the conditions of 25 °C, a loading rate of 5 mm/min and a notch depth of 10–15 mm are proposed as the routine ambient-temperature cracking-resistance condition for the SCB test: under these conditions, the material is dominated by elastoplastic deformation, cracks propagate stably along the binder for easy

observation, test efficiency is moderate, and the cracking resistance of different asphalt mixtures can be well distinguished.

The findings of this study provide a reference for selecting cracking resistance evaluation methods and optimizing test parameters. However, because the three methods were compared at −10 °C under different loading rates, specimen geometries, loading configurations and fracture mechanisms, the differences cannot be attributed solely to the test method; the comparative conclusions apply to the specific procedures used rather than to the general reliability of the methods. Moreover, only three AC-13 mixtures with essentially identical gradation were tested, the parameter analysis was conducted mainly on the SBS-modified mixture, and the proposed conditions were not verified for other mixtures or against actual pavement cracking. With a limited number of parallel specimens per condition, the repeatability of the energy indices was not fully evaluated. Future work should verify the proposed conditions on more mixture types under harmonized loading, including field validation, further explore the rate–temperature coupling of fracture energy, and report the scatter of the energy indices on adequately replicated specimens.

Author Contributions: Conceptualization, F.H. and H.R.; Methodology, F.H., F.X. and H.R.; Software, C.J., K.L. and X.Y.; Validation, C.J., F.X. and H.R.; Formal analysis, C.J., D.Y. and K.L.; Investigation, B.W., K.L. and X.Y.; Resources, B.W., D.Y. and X.Y.; Data curation, D.Y.; Writing—original draft, F.H.; Writing—review & editing, F.H.; Visualization, B.W.; Supervision, B.W. and H.R.; Project administration, F.X. All authors have read and agreed to the published version of the manuscript.

Funding: This research was funded by the Science and Technology Projects of Xizang Autonomous Region, China (grant numbers XZ202501JD0008 and XZ202601ZY0020).

Institutional Review Board Statement: Not applicable.

Informed Consent Statement: Not applicable.

Data Availability Statement: The data presented in this study are available on request from the corresponding author.

Conflicts of Interest: Authors Feng Huang, Can Jiang, Binbin Wang, Desheng Yang, Feng Xiong and Xin Yuan were employed by the company China Merchants Zhixiang Road Technology (Chongqing) Co., Ltd. Authors Feng Huang, Binbin Wang and Desheng Yang were employed by China Merchants Chongqing Communications Technology Research and Design Institute Co., Ltd. The remaining authors declare that the research was conducted in the absence of any commercial or financial relationships that could be construed as a potential conflict of interest.

References

1. Ren, J.; Sun, L. Characterizing Air Void Effect on Fracture of Asphalt Concrete at Low-Temperature Using Discrete Element Method. *Eng. Fract. Mech.* **2017**, *170*, 23–43. [CrossRef]
2. Huang, X.; Gao, Y. *Principles and Methods of Pavement Design*; China Communications Press: Beijing, China, 2015. (In Chinese)
3. Ling, T. *Road Engineering*; China Communications Press Co., Ltd.: Beijing, China, 2016; p. 187. (In Chinese)
4. Zheng, J.; Zhou, Z.; Zhang, Q. *Theory and Method of Anti-Cracking Design for Asphalt Pavements*; China Communications Press: Beijing, China, 2003. (In Chinese)
5. Zhang, X. *Viscoelastic Mechanics of Asphalt and Asphalt Mixtures*; China Communications Press Co., Ltd.: Beijing, China, 2006. (In Chinese)
6. Kaseer, F.; Yin, F.; Arámbula-Mercado, E.; Martin, A.E. Development of an Index to Evaluate the Cracking Potential of Asphalt Mixtures Using the Semi-Circular Bending Test. *Constr. Build. Mater.* **2018**, *167*, 286–298. [CrossRef]
7. Zhang, X.; Han, C.; Zhu, X. Study on Evaluation Method of Low-Temperature Anti-Cracking Performance of Asphalt Mixtures. *China J. Highw. Transp.* **1999**, *6*, 3–9. (In Chinese)
8. Ge, Z.; Huang, X.; Xu, G. Evaluation of Low-Temperature Anti-Cracking Performance of Asphalt Mixtures by Bending Strain Energy Method. *J. Highw. Transp. Res. Dev.* **2002**, *32*, 653–655. (In Chinese)
9. Shen, A.; Jiang, Q. Evaluation and Influencing Factors of Low-Temperature Anti-Cracking Performance of Asphalt Mixtures. *J. Chang'an Univ. Nat. Sci. Ed.* **2004**, *24*, 1–6. (In Chinese)

10. Kim, H.; Wagoner, M.P.; Buttlar, W.G. Micromechanical Fracture Modeling of Asphalt Concrete Using a Single-Edge Notched Beam Test. *Mater. Struct.* **2009**, *42*, 677–689. [CrossRef]
11. Wagoner, M.P.; Buttlar, W.G.; Paulino, G.H. Development of a Single-Edge Notched Beam Test for Asphalt Concrete Mixtures. *J. Test. Eval.* **2005**, *33*, 452–460. [CrossRef]
12. Yin, F.; Garita, J.; Taylor, A.; Turos, M.; Marasteanu, M. Refining the Indirect Tensile (IDT) Nflex Factor Test to Evaluate Cracking Resistance of Asphalt Mixtures for Mix Design and Quality Assurance. *Constr. Build. Mater.* **2018**, *172*, 396–405. [CrossRef]
13. Pi, Y.; Zhang, J.; Huang, X.; Qian, Z. Numerical Simulation of Asphalt Splitting Test. *J. Highw. Transp. Res. Dev.* **2007**, *24*, 1–6. (In Chinese)
14. Krans, R.L.; Tolman, F.; Van de Ven, M.F.C. Semi-Circular Bending Test: A Practical Crack Growth Test Using Asphalt Concrete Cores. In Proceedings of the International RILEM Conference on Reflective Cracking in Pavements, Nijmegen, The Netherlands, 2–4 October 1996.
15. Zeng, G.; Yang, X.; Chen, L.; Sun, Y. Damage Evolution and Crack Propagation in Semicircular Bending Asphalt Mixture Specimens. *Acta Mech. Solida Sin.* **2016**, *29*, 596–609. [CrossRef]
16. Lancaster, I.M.; Khalid, H.A.; Kougioumtzoglou, I.A. Extended FEM Modelling of Crack Propagation Using the Semi-Circular Bending Test. *Constr. Build. Mater.* **2013**, *48*, 270–277. [CrossRef]
17. Al-Qudsi, A.; Cannone Falchetto, A.; Wang, D.; Wistuba, M.P. Finite Element Cohesive Fracture Modeling of Asphalt Mixture Based on the Semi-Circular Bending (SCB) Test and Self-Affine Fractal Cracks at Low Temperatures. *Cold Reg. Sci. Technol.* **2020**, *169*, 102913. [CrossRef]
18. Ozer, H.; Al-Qadi, I.L.; Lambros, J.; El-Khatib, A.; Singhvi, P.; Rivera-Perez, J. Development of the Fracture-Based Flexibility Index for Asphalt Concrete Cracking Potential Using Modified Semi-Circle Bending Test Parameters. *Constr. Build. Mater.* **2016**, *115*, 390–401. [CrossRef]
19. Razmi, A.; Mirsayar, M.M. Fracture Resistance of Asphalt Concrete Modified with Crumb Rubber at Low Temperatures. *Int. J. Pavement Res. Technol.* **2018**, *11*, 265–273. [CrossRef]
20. Some, S.C.; Fredj, M.A.; Nguyen, M.L.; Delaplace, A. Multi-Parametric Characterization of Mode I Fracture Toughness of Asphalt Concrete: Influence of Void and RA Contents, Binder and Aggregate Types. *Int. J. Pavement Res. Technol.* **2018**, *11*, 274–284. [CrossRef]
21. Some, S.C.; Feeser, A.; Pavoine, A. Numerical and Experimental Investigation of Mode I Cracking of Asphalt Concrete Using Semi-Circular Bending Test. *Constr. Build. Mater.* **2018**, *169*, 34–46. [CrossRef]
22. Aliha, M.R.M.; Fazaeli, H.; Aghajani, S.; Moniri, A. Effect of Temperature and Air Void on Mixed Mode Fracture Toughness of Modified Asphalt Mixtures. *Constr. Build. Mater.* **2015**, *95*, 545–555. [CrossRef]
23. Pirmohammad, S.; Ayatollahi, M.R. Fracture Resistance of Asphalt Concrete Under Different Loading Modes and Temperature Conditions. *Constr. Build. Mater.* **2014**, *53*, 235–242. [CrossRef]
24. Huang, B.; Shu, X.; Tang, Y. Comparison of Semi-Circular Bending and Indirect Tensile Strength Tests for HMA Mixtures. In *Advances in Pavement Engineering, Proceedings of the GeoFrontiers 2005 Austin, TX, USA, 24–26 January 2005*; ASCE: Reston, VA, USA, 2005; pp. 1–12.
25. *EN 12697-44:2019*; Bituminous Mixtures—Test Methods for Hot Mix Asphalt—Part 44: Crack Propagation by Semi-Circular Bending Test. European Committee for Standardization: Brussels, Belgium, 2019.
26. *AASHTO TP 124*; Standard Method of Test for Determining the Fracture Potential of Asphalt Mixtures Using the Illinois Flexibility Index Test (I-FIT). American Association of State Highway and Transportation Officials: Washington, DC, USA, 2020.
27. Kim, M.; Mohammad, L.N.; Elseifi, M.A. Characterization of Fracture Properties of Asphalt Mixtures as Measured by Semicircular Bend Test and Indirect Tension Test. *Transp. Res. Rec.* **2012**, *2296*, 115–124. [CrossRef]
28. Saha, G.; Biligiri, K.P. Fracture Properties of Asphalt Mixtures Using Semi-Circular Bending Test: A State-of-the-Art Review and Future Research. *Constr. Build. Mater.* **2016**, *105*, 103–112. [CrossRef]
29. Zhang, J.; Tan, H.; Pei, J.; Qu, T.; Liu, W. Evaluating Crack Resistance of Asphalt Mixture Based on Essential Fracture Energy and Fracture Toughness. *Int. J. Geomech.* **2019**, *19*, 06019005. [CrossRef]
30. *JTG E20—2011*; Standard Test Methods of Bitumen and Bituminous Mixtures for Highway Engineering. Industry Standard of the People's Republic of China: Beijing, China, 2011. (In Chinese)
31. *JTG F40—2004*; Technical Specifications for Construction of Highway Asphalt Pavements. Industry Standard of the People's Republic of China: Beijing, China, 2004. (In Chinese)
32. *JTG E42—2005*; Test Methods of Aggregate for Highway Engineering. Industry Standard of the People's Republic of China: Beijing, China, 2005. (In Chinese)
33. Hofman, R.; Oosterbaan, B.; Erkens, S.; van der Kooij, J. Semi-Circular Bending Test to Assess the Resistance Against Crack Growth. In Proceedings of the 6th RILEM Symposium on Performance Testing and Evaluation of Bituminous Materials, Zurich, Switzerland, 14–16 April 2003; pp. 257–263.

34. Abdulshafi, A.A.; Majidzadeh, K. J-Integral and Cyclic Plasticity Approach to Fatigue and Fracture of Asphalt Mixtures. In Proceedings of the 64th Annual Meeting of the Transportation Research Board, Washington, DC, USA, 14–18 January 1985; pp. 112–123.
35. Doll, B.; Ozer, H.; Rivera-Perez, J.; Al-Qadi, I.L.; Lambros, J. Fracture Process Zone Development in Heterogeneous Asphalt Concrete. *Eng. Fract. Mech.* **2017**, *182*, 356–371. [CrossRef]
36. Zegeye, E.; Le, J.-L.; Turos, M.; Marasteanu, M. Investigation of Size Effect in Asphalt Mixture Fracture Testing at Low Temperature. *Road Mater. Pavement Des.* **2012**, *13*, 88–101. [CrossRef]

Disclaimer/Publisher's Note: The statements, opinions and data contained in all publications are solely those of the individual author(s) and contributor(s) and not of MDPI and/or the editor(s). MDPI and/or the editor(s) disclaim responsibility for any injury to people or property resulting from any ideas, methods, instructions or products referred to in the content.